



Liquid metal/CNT nanocomposite coated cotton fabrics for electromagnetic interference shielding and thermal management

Junsheng Wang · Yong Wang · Rao Jue · Daiqi Li · Zhong Zhao · Guangming Cai · Deshan Cheng · Xin Wang

Received: 29 June 2022 / Accepted: 23 August 2022 / Published online: 31 August 2022
© The Author(s), under exclusive licence to Springer Nature B.V. 2022

Abstract Next-generation smart textiles are regarded as the most straightforward and effective solution to address the growing threats from environment including excessive electromagnetic radiation and global warming. Incorporation of novel materials using advanced fabrication technology has been the reliable technology in developing these smart textiles. Herein, a novel fabrication strategy integrating multi-layer spraying and mechanical compression is proposed to fabricate a liquid metal (LM) and carbon nanotubes (CNT)-decorated multi-functional cotton fabric (CF/LM/CNT). The results demonstrate that the double face-sprayed CF/LM/CNT possess electrical resistance of 0.07 Ω , which

is primarily responsible for its unprecedented electromagnetic shielding effectiveness of about 85 dB over the X-band. Moreover, the CF/LM/CNT exhibits excellent heat dissipation and thermal insulation behavior, which is an essential prerequisite for effective thermal management. More importantly, the as-prepared CF/LM/CNT is recycled and reconfigured. This fundamental research work provides a facile and scalable approach to fabricate multifunctional textile materials.

Keywords Cotton fabric · Liquid metal · Carbon nanotube · Spraying · Electromagnetic interference shielding · Thermal management

Junsheng Wang and Yong Wang equally contributed to this work.

J. Wang · Y. Wang · R. Jue · D. Li · Z. Zhao · G. Cai · D. Cheng
State Key Laboratory of New Textile Materials and Advanced Processing Technologies, Wuhan Textile University, Wuhan 430073, China

J. Wang · R. Jue (✉) · D. Li · Z. Zhao (✉) · G. Cai · D. Cheng (✉)
School of Textile Science and Engineering, Wuhan Textile University, Wuhan 430200, China
e-mail: raojue@wtu.edu.cn

Z. Zhao
e-mail: zzhao@wtu.edu.cn

D. Cheng
e-mail: chengcds@163.com

Y. Wang
College of Textiles and Garments, Anhui Polytechnic University, Wuhu 241004, China

D. Cheng
Jiangsu R&D Center of the Ecological Textile Engineering & Technology, Yancheng Polytechnic College, Yancheng 224005, China

X. Wang
School of Fashion and Textiles, RMIT University, Melbourne 3056, Australia

Introduction

Electromagnetic interference (EMI) and excessive heat from massive use of electronic equipment is a big concern posing threats to human health and possible danger, e.g., fire (Lee et al. 2016; Bhattacharjee et al. 2018; Yang et al. 2020). Therefore, there is an urgent need to develop electromagnetic shielding materials with excellent heat dissipation ability. Metals with conductive and heat-conducting functions are the preferred materials to achieve excellent electromagnetic shielding, but their high density, poor anti-oxidant properties, difficulty in processing and easy to be contaminated by secondary reflection limit their practical application (Sankaran et al. 2018; Wang et al. 2021; Hao et al. 2022).

In recent years, liquid metals (LMs) have shown a great application potential in the field of EMI shielding due to their good machinability and excellent thermal conductivity. Liao et al. provided a novel strategy including ball-milling dispersion, freeze-drying and compression molding to prepare LM/cellulose nanofiber composites for electromagnetic shielding properties (Liao et al. 2021). Yu et al. prepared a stretchable LM foam elastomer with the electromagnetic shielding value increased from 48 to 83 dB under tensile deformation (Yu et al. 2020). Yao et al. developed a flexible composite material by introducing three-dimensional liquid metal networks into elastomeric foams, which exhibited significantly increased electromagnetic shielding effects under compression (Yao et al. 2021). Zhang et al. produced porous and anisotropic liquid metal matrix composites as low temperature electromagnetic shielding materials (Zhang et al. 2020). However, the application of LM in EMI shielding is seriously hampered by its high surface tension, insulated oxide shells formed during processing and uncontrollable flowability (Dobosz et al. 2021; Mwesigye and Yılmaz 2020). Therefore, large-scale processing of flexible LM materials with encapsulation capacity and excellent electromagnetic shielding remains a great challenge.

Textiles as the interface between human and environment is a perfect substrate for developing EMI and thermal management for protecting human (Mondal et al. 2017; Cheng et al. 2020a, b; Xu et al. 2021; Guo et al. 2021). Textiles are flexible and friendly to human and well-settled in human civilization. However, the intrinsic properties of textiles result in poor

EMI and thermal management performance. Recent years have seen great advances in developing nanocomposite textiles with the application potential in smart textiles including EMI and thermal management. Novel active nanomaterials such as CNT and graphene have grown great potential in developing the next-generation textiles (Ji et al. 2014; Cheng et al. 2020c; Chen et al. 2021). Searching for other novel materials to bring new functions, such as EMI and protection, is always on the agenda of developing protective clothing.

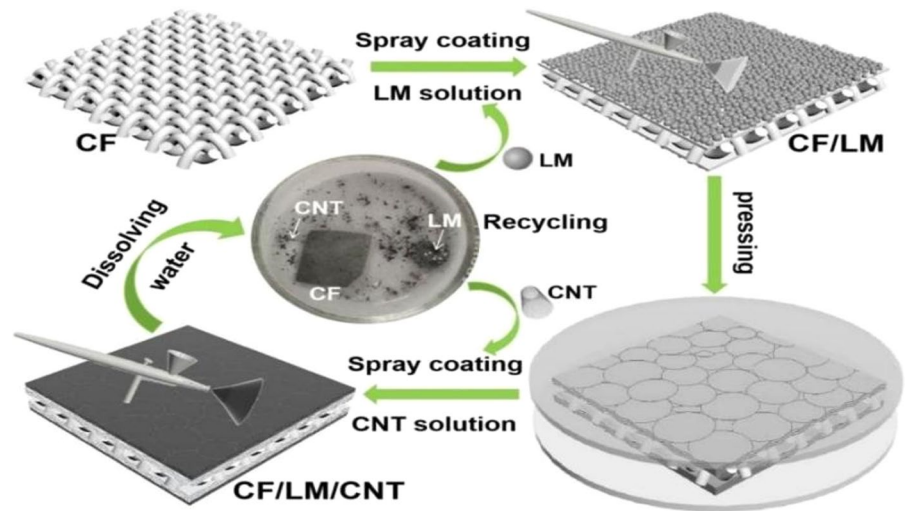
Here, EMI shielding fabrics with excellent heat dissipation properties from liquid metals (LM) and carbon nanotubes (CNTs) are fabricated by simple spray-assisted mechanical pressure. The presence of CNT plays an encapsulation role to prevent the oxidation of LM. Interestingly, the LM is impregnated into the yarn under auxiliary mechanical pressure, which not only fills the inter fiber gap and form a highly conductive LM “network cake”. The CF/LM/CNT has an extremely high conductivity with an EMI SE of 68 dB only at 20 μm thickness. In addition, the heat dissipation and heat insulation of fabrics coated with LM/CNT were studied. Finally, LM and CNT can be recycled from CF/LM/CNT to solve the problem of e-waste recycling. This work provides new strategies of developing recyclable electromagnetic shielding materials for future development of recyclable electronic products.

Experimental

Materials

A pure cotton woven fabric (plain weave, 135 g/m^2) was purchased from Wuhan Yudahua Textile Co., Ltd., China. It was washed and cleaned with acetone and deionized water before using, and then dried in an oven at 60 $^\circ\text{C}$. The eutectic gallium-indium liquid metal (LM, 75.5% Ga and 24.5% In, by weight; melting point of 16 $^\circ\text{C}$) was purchased from Dongguan Dingguan Metal Technology Co., Ltd., China. The carbon nanotube solution (0.15 wt%) was purchased from Nanjing Xianfeng Nanomaterials Technology Co., Ltd., China. Note that all the chemicals are analytical grade and were used without further purification.

Fig. 1 Diagram of the preparation procedures of the CF/LM/CNT



Preparation of CF/LM/CNT

The schematic of fabrication procedure of a CF/LM/CNT fabric is graphically illustrated in Fig. 1. Firstly, 2 g of LM was ultrasonically dispersed in 10 mL ethanol solution followed by spraying onto CF and using hairdryer to dry. The resultant dried fabric was marked as CF/LM. Secondly, the dried CF/LM sample was mechanically pressed under a pressure of 1 MPa for 2 min at room temperature. Finally, a CNT solution (20 mL, 0.15 wt%) was sprayed onto the pressed CF/LM followed by oven drying. The single-side LM/CNT-decorated CF was marked as CF/LM/CNT-S. In addition, the fabric sample with double side coating LM and CNT (i.e., CF/LM/CNT-D) were prepared for comparison. Note that if not otherwise specified the fabric of CF/LM/CNT-S was abbreviated as CF/LM/CNT.

Characterization of the CF/LM/CNT

The surface morphology and chemical element of the sprayed fabric sample were determined using scanning electron microscopy (SEM, JSM-5600LV, JEOL, Japan) equipped with energy dispersive X-ray spectroscopy (EDS, Oxford Instruments, Oxford, UK). Specifically, the samples were cut into the same dimensions of 5×5 mm. To further enhance the conductivity of the samples during the scanning, all the samples were coated with Au via sputtering deposition. The accelerating voltage applied in the scanning process was 15 kV. The crystal structure of the

fabric samples was measured by scanning them with the X-ray (with the wavelength of 0.154 nm) generated by a Cu $K\alpha$ radiation source of an X-ray powder diffractometer (XRD) analyzer (D/MAX 2500 type) in the reflection mode. To eliminate the possible phase change of the LM, the samples were cut into the dimensions of 2×2 cm and directly fixed in the sample holder for XRD scanning without further processing. The surface chemical state of as-prepared fabric was characterized by X-ray photoelectron spectroscopy (XPS, Perkin-Elmer, PHI 5000 C, America). The samples were cut into the dimensions of 5×5 mm and mounted on a sample holder without further treatment prior to the XPS tests. The electrical resistance of fabric sample with an electrode gap of 1 cm was tested by resistance meter (CHI604E Instruments, China) and each specimen was tested 10 times.

Electromagnetic shielding measurement

The electromagnetic shielding effectiveness (EMSE) performance of various fabric samples was investigated in X-band (8.2–12.4 GHz) frequency range. Measurements were made over the X-band range using a vector network analyzer (VNA; Rohde & Schwarz ZVL6). The samples were prepared to a geometric shape ($4 \text{ cm} \times 3 \text{ cm}$) to fit the waveguide. Prior to the tests, a Thru-Reflect-Line (TRL) calibration was performed in order to remove the errors. The S -parameters (S_{11} , S_{12} , S_{22} and S_{21}) were recorded. Based on the above S -parameters, the total EMSE, absorption, reflection (i.e., SE_T , SE_A , SE_R),

and the coefficient of transmissivity, reflectivity and absorptivity (i.e., T , R , A) could be calculated and given. Five replicates were tested for each sample, and the average value of each sample was obtained accordingly.

Thermal performance measurement

A self-designed experimental setup was built to investigate the heat dissipation behavior of the fabric samples. The setup consists of three parts: a thermal imager connected to a phone, a matrix of LED lights, and a power supply (see Fig. 6a). The fabric sample with an exact size of 4 cm × 3 cm was placed onto the surface of the matrix of LED lights, and then the LED lights were heated by controlling the voltage of 18 V of the power supply. The heating process would be stopped when the temperature of fabrics reached the predetermined value. Meanwhile, the temperature change of the fabrics during the dissipating process was real-time monitored by a thermal imager, and finally, the curve (temperature vs. time) of each fabric can be plotted.

Further, a self-designed experimental setup was built to investigate the thermal insulation behavior of the fabric samples. The setup consists of two parts: a thermal imager connected to a phone, and a hot plate whose temperature can be precisely controlled (see Fig. 7a). The two fabric samples with the exact size of 4 cm × 3 cm were tightly contacted with the surface of the hot plate (with initial temperature of 50 °C). Similarly, the temperature change of the fabrics during the experimental process was real-time monitored by a thermal imager, and the curve (temperature vs. time) of each fabric was plotted.

Results and discussion

Characterization of CF/LM/CNT

The SEM-EDS images of as prepared CF/LM/CNT are presented in Fig. 2. As shown in Fig. 2a, the appearance colors of the pristine CF, CF/LM, and CF/LM/CNT are white, silvery and black, respectively. Further, the overall and partially enlarged SEM images of the pristine CF were shown in Fig. 2b, c. The CF with plain weave can be seen in Fig. 2b, and the micro-grooves of CF can be observed (see

Fig. 2c). The surface morphology of LM/CF is presented in Fig. 2d, e. The LM component has been tightly attached to the fabric surface, and the LM units in irregular cake shape with inter-connection to each other. Figure 2f, g present the appearance of CF/LM/CNT. The CNTs are uniformly attached onto the LM as suggested by Fig. 2g. The CNTs layer play a key role in encapsulating the liquid metal and preventing its oxidation. Figure 2h shows the cross-section of CF/LM/CNT. A typical three-layered CF/LM/CNT fabric sample can be observed, and the components of the top, middle and bottom layers are CNTs, LM and CF, respectively. In addition, Fig. 2i displays the EDS spectrum of as-prepared CF/LM/CNT. Four elements (i.e., C, O, Ca and In) can be detected from the spectrum (as summarized in the inset table), and the proportions of the four elements are 26.32%, 12.80%, 51.17% and 9.71%, respectively.

The crystal structure of both CF, CF/LM, and CF/LM/CNT was investigated by X-ray diffraction analysis. Figure 3a illustrates the typical XRD spectra of the three fabric samples. Pristine CF exhibits four significant characteristic peaks around 14.5°, 16.1°, 22.4° and 33.7°, corresponding to the crystal faces (1–10), (110), (200), and (004) of cellulose I β , respectively (Cheng et al. 2018; Ran et al. 2020). As for CF/LM and CF/LM/CNT fabrics, a broad characteristic peak around 35.0° corresponding to the liquid metal is detected (Wei et al. 2019; Luo et al. 2020). At the same time, the characteristic peaks of the cotton are weakened. Figure 3b shows the XRD pattern of CF/LM/CNT. Due to the introduction of CNT, a new characteristic peak at 26.5° indexed to the (002) facet of graphitic carbon can be observed (Hu et al. 2014; Dong et al. 2020). The above analysis reveals that the LM and CNT have been successfully loaded onto the surface of the pristine CF.

X-ray photoelectron spectroscopy (XPS) analysis of the CF/LM/CNT fabric surface was also performed. The wide scan XPS spectrum of the CF/LM/CNT is shown in Fig. 3c. Except for C1s and O1s peaks, some extra peaks of Ga and In have been detected. For Ga 3d spectrum (Fig. 3d), three obvious peaks can be found. The characteristic peaks at around 16.8 eV, 18.5 eV, and 20.3 eV are assigned to In 4d, Ga and Ga₂O₃, respectively (Peng et al. 2016). The intensity peaks of Ga₂O₃ can also be observed, indicating that part of the Ga metal has been oxidized into Ga₂O₃ (He et al. 2021). This is because

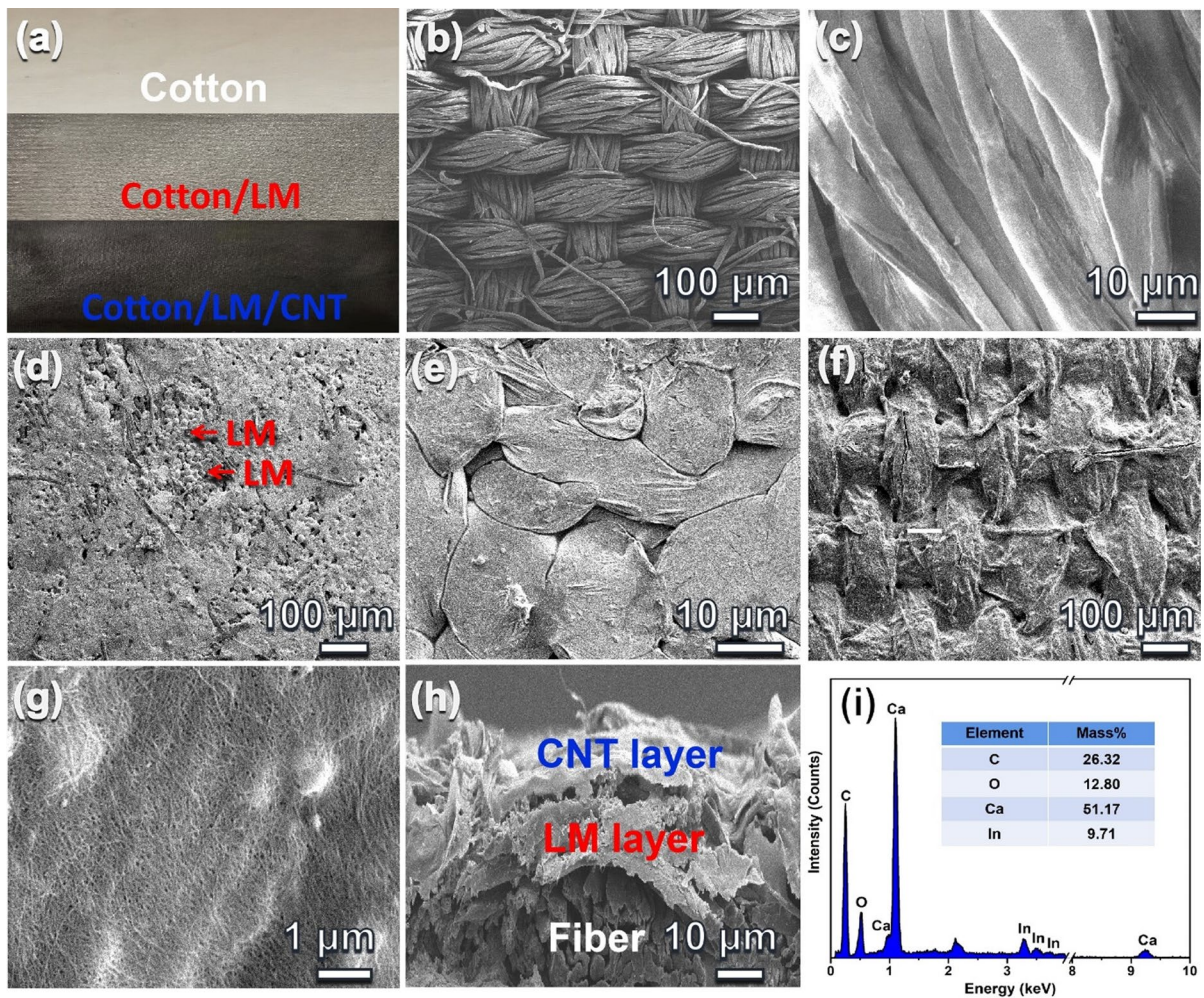


Fig. 2 Optical photos (a) and SEM images of CF (b, c), CF/LM (d, e), CF/LM/CNT (f, h) and EDS spectra (i) (Bar = 100 μm and 10 μm for overview and magnified view SEM images, respectively)

when LM is exposed to air, its surface can be easily oxidized to a thin Ga_2O_3 layer. The XPS spectrum for In 3d (Fig. 3e) consists of two peaks at 444 eV and 445 eV relating to In and In_2O_3 , respectively (Guo et al. 2019). The XPS of C 1s could be deconvoluted into three peaks at 284.8 eV, 286.3 eV and 287.4 eV, attributing to C–C, C–O and C=O, respectively (Fig. 3f) (Bi et al. 2021). These XPS results further confirm that the LM and CNT have been successfully loaded onto the surface of CF.

Electromagnetic shielding performance

Owing to the excellent electrical conductivity of LM and CNT, the as-prepared CF/LM/CNT has shown a

broad application potential in electromagnetic shielding field. As shown in Fig. 4a, the pure CF is non-conductive because the cotton fiber is an electrical insulator. With LM and LM/CNT sprayed on the fabric surface separately, the electrical resistance of the coated fabric was 0.84 and 0.07 Ω , respectively (Fig. 4a). It is evident that LM or LM/CNT has a high electrical conductivity.

Figure 4b shows the results of EMSE of different fabric samples (i.e., CF/LM/CNT-D, CF/LM/CNT-S, CF/LM and CF) over the X-band. The results indicate that all the coated fabrics are effective for electromagnetic shielding purpose, and the EMSE of the coated fabrics is dependent on the types and contents of the coated components. In comparison, the CF/

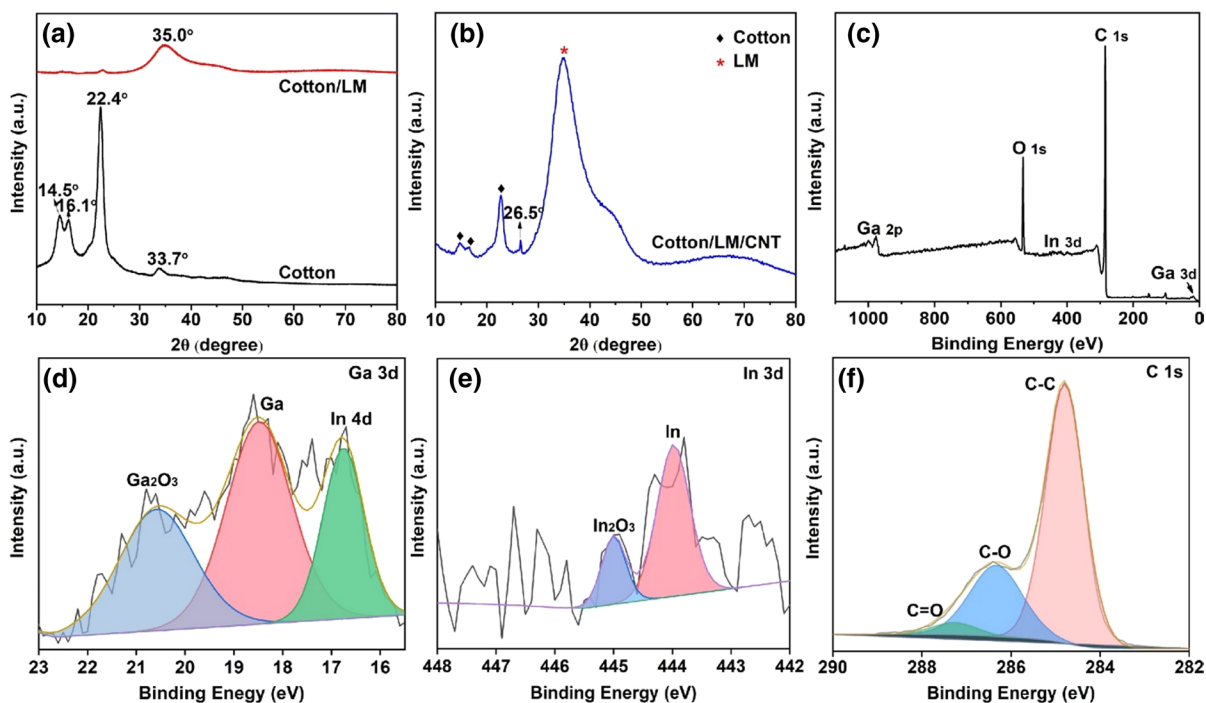


Fig. 3 Whole (a) and partial enlarged XRD patterns (b) of CF/LM/CNT and CF/LM samples; c The wide scan XPS spectrum of the CF/LM/CNT; d–f High resolution XPS spectra of Ga 3d, In 3d, and C 1s, respectively

LM/CNT-D has the best EMSE capability with an EMSE value of about 85 dB, followed by CF/LM/CNT-S (about 68 dB) and CF/LM (about 54 dB). As expected, the EMSE of CF is almost zero because the cotton fiber is an electrical insulator, therefore it is transparent to the electromagnetic radiation. Furthermore, the response to the frequency across the EMSE of the three coated fabric samples is also presented in Fig. 4b. The value of EMSE generally decreases with the increase of frequency over the X-band. This result reveals that the EMSE capability of electromagnetic shielding fabrics is slightly higher for lower-frequency/longer waves than for higher-frequency/shorter waves.

Taking the frequency of 9 GHz for example, it is apparent from Fig. 4c, d that the EMSE of CF is only about 0.366 dB, whereas that for CF/LM, CF/LM/CNT-S, and CF/LM/CNT-D is 53.66, 68.31 and 84.89 dB, respectively. Furthermore, the SE_A was always higher than the SE_R from CF/LM to CF/LM/CNT samples irrespective of single or double coated considered. As a proof-of-concept, we

constructed a simple device by employing a Tesla coil and a green light-emitting diode (LED), as shown in Fig. 4e–g. Herein, our prepared CF/LM/CNT was used to demonstrate its electromagnetic shielding capacity. The Tesla coil will radiate high frequency electromagnetic waves. When the CF fabric sample was placed in between the coil and LED, the LED remains on. When the CF/LM/CNT was introduced, the LED was off immediately, and it returned to illuminated immediately when removing the CF/LM/CNT. The process can be repeated for many times with confidence. This result reveals the excellent electromagnetic shielding capacity of the as-prepared CF/LM/CNT. Further, a comparison of the total value SE_T and main shielding mechanism with other reported available electromagnetic shielding materials is given in Table 1. The as-prepared CF/LM/CNT exhibits outstanding electromagnetic shielding capability over X-band when compared to currently available fabric-based EMI shielding materials.

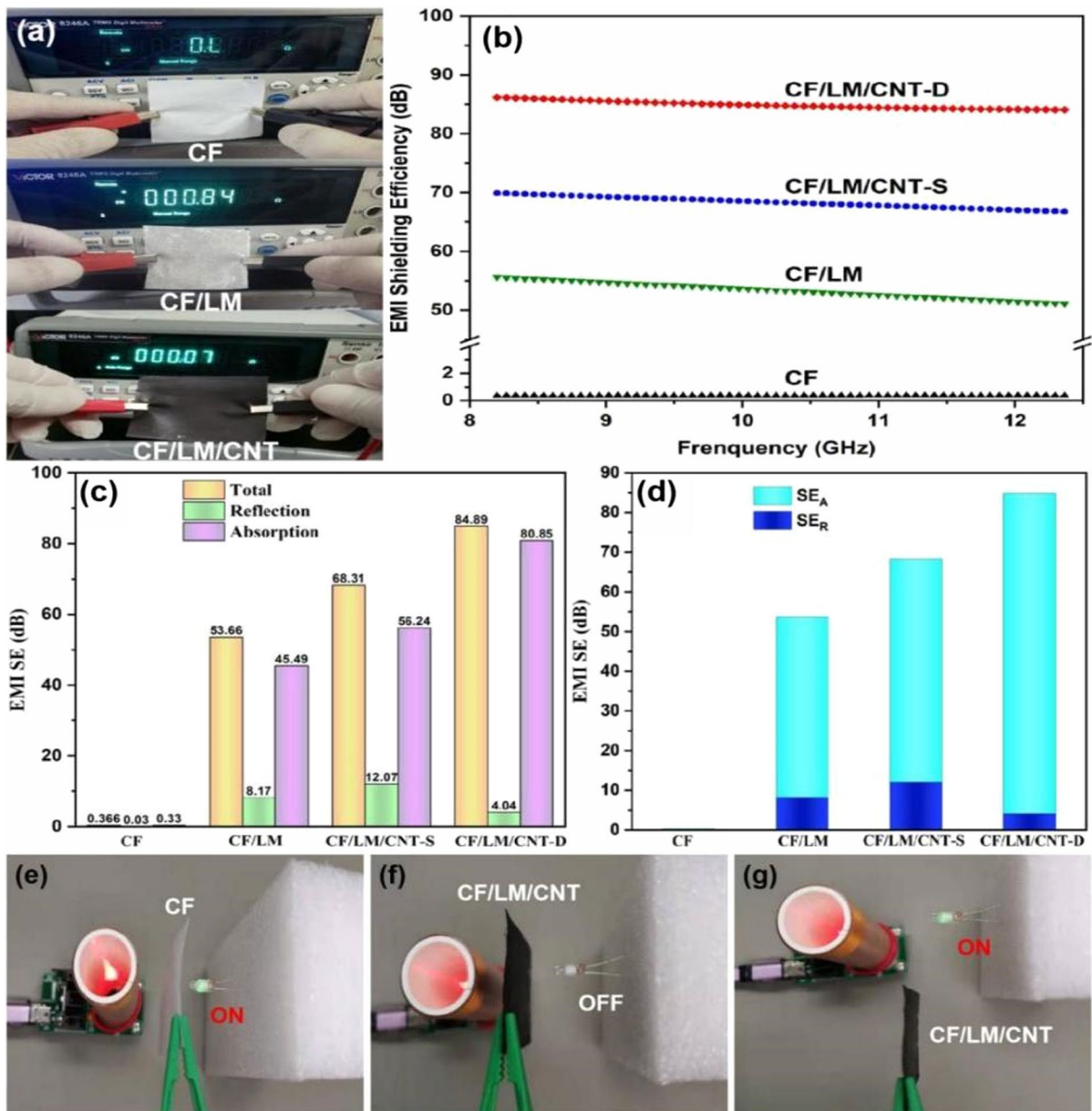


Fig. 4 **a** Comparison of the electrical resistance of CF, CF/LM and CF/LM/CNT samples; **b** Total EMSE of CF/LM/CNT-D, CF/LM/CNT-S, CF/LM and CF samples over the X-band; **c**, **d** The contributions from absorption SE_A and

reflection SE_R to the total SE_T of CF/LM, CF/LM/CNT-S, CF/LM/CNT-S at frequency of 9 GHz; **e–g** Comparison of CF/LM/CNT and CF used as an electromagnetic barrier material

Electromagnetic shielding mechanism

The underlying electromagnetic shielding mechanism of the as-prepared multilayer CF/LM/CNT-D fabric is graphically illustrated in Fig. 5. When the electromagnetic waves reach to the carbon nanotube layer on

the surface of the fabric, a part of the incident waves reflect while the others enter the fabric (i.e., the liquid metal layer). Since the liquid metal layer has a multilayer structure, the entered waves will be reflected and absorbed many times, leading to attenuation of the waves. Furthermore, when the transmitted waves

Table 1 Comparison of the total value SE_T and main shielding mechanism of fabric-based electromagnetic shielding materials

Fabrics	SE_T (dB)	Frequency (GHz)	Main shielding mechanism	Refs.
CF/PPy/Cu	30–50	0.03–1	Reflection	Zhao et al. (2016)
PANI/Co-Ni coated LyF	34–46	8.2–12.4	Reflection	Zhao et al. (2017)
Cu plated PET	40–50	6–18	Reflection	Qin and Guo (2015)
Fe-Si-B/Ni-Cu-P	~40	8.2–12.4	Absorption	Zhang et al. (2017)
50Ni-Co-Fe-P/PANI/P	69.4	8.2–12.4	Absorption	Wang et al. (2020)
PP/Ag/mCNTs	61.1	8.2–12.4	Absorption	Hu and Kang (2021)
CF/LM/CNT-S	68	8.2–12.4	Absorption	This work
CF/LM/CNT-D	85	8.2–12.4	Absorption	This work

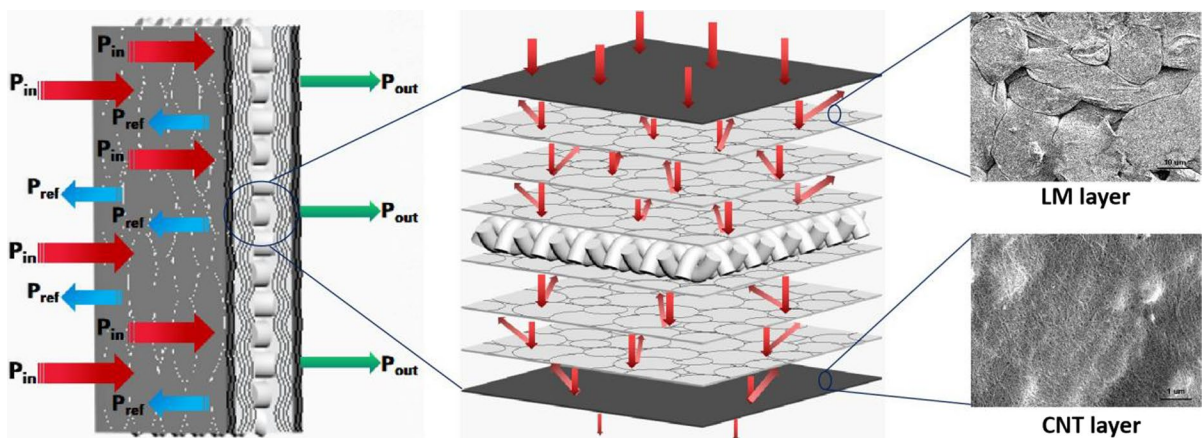


Fig. 5 The underlying electromagnetic shielding mechanism of the as-prepared CF/LM/CNT

pass through the last cotton layer, the reflection, absorption as well as transmission will take place. Finally, only few electromagnetic waves will pass through the thickness direction of the multi-layer CF/LM/CNT fabric. In addition, the mechanical pressure have a beneficial effect on the EMI shielding of fabric, because the gaps in the fabric were filled with LM.

Thermal management performance

An experimental setup was developed to study the heat dissipation behavior of CF/LM/CNT fabric. As illustrated in Fig. 6a, the instrument consists of three parts, i.e., a thermal imager connected to a phone, a matrix of LED lights, and a power supply. The fabric was placed onto the surface of the matrix of LED lights, and the fabric temperature can be precisely

controlled by the combination of a power supply and the matrix of LED lights. Here, the initial temperature of fabric is set to 50 °C. In addition, the temperature change of fabric during the dissipating process was monitored by a thermal imager. Figure 6b shows the heat dissipation curves of pure CF and CF/LM/CNT. The surface temperature of the two fabrics decreased as a function of time, and the temperature dropped severely in the beginning followed by gradually slow declining irrespective of the fabrics considered. In comparison, the temperature drop rate of CF/LM/CNT fabric is higher than that of the CF fabric. The captured images of two fabrics at varying times have confirmed this difference, as shown in Fig. 6c. The temperature of CF dropped to 39.8 °C at 12 s, whereas for the CF/LM/CNT fabric it was 32.5 °C. The above analysis demonstrated that the prepared CF/LM/CNT fabric has excellent heat dissipating performance.

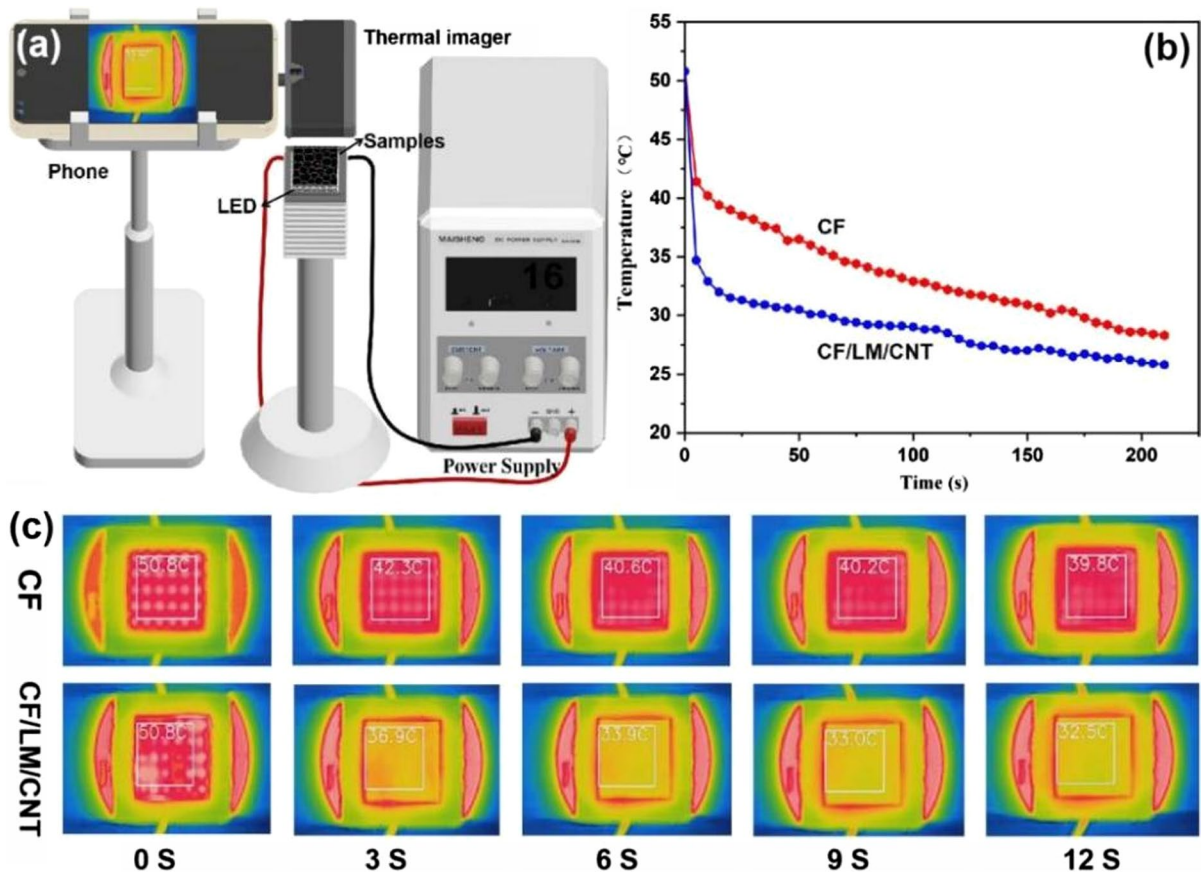


Fig. 6 **a** A self-designed experimental setup for investigating the heat dissipation behavior of CF/LM/CNT; **b** Comparison of the heat dissipation curves of CF/LM/CNT and CF samples; **c** The captured infrared images of CF/LM/CNT and CF at varying times

Another experimental device was established to investigate the thermal insulation behavior of CF/LM/CNT fabric. As illustrated in Fig. 7a, the instrument consists of a thermal imager connected to a phone and a hot plate with its temperature precisely controllable. The prepared CF/LM/CNT and CF were tightly attached to the surface of hot plate at an initial temperature of 50 °C, and the temperature changes of the two fabrics during the experimental process were monitored by the thermal imager. Figure 7b shows the thermal insulation curves of pure CF and CF/LM/CNT at the same time intervals. The fabric temperature gradually increased as a function of time, but the rate of temperature rise was obviously different. The captured images of two fabrics at different time intervals have confirmed this difference (see Fig. 7c). The CF/LM/CNT has excellent thermal insulation performance with the temperature increasing less than

5 °C within 20 s. However, the temperature for CF increased more than 10 °C within the same 20 s. The excellent thermal insulation capacity of CF/LM/CNT is due to its special multilayer structure with prominent absorption and reflection of thermal radiation across the thickness. The incoming thermal radiation from the hot plate will be absorbed and reflected by the CNT and LM layers, and thus only part of heat will finally reach the outside surface. In short, the as-prepared CF/LM/CNT fabric has excellent thermal insulation performance.

Recycling performance

Electronic waste as a thorny issue has been affecting the environment and the economy, so it is very important to realize the reconfiguration and recycling of electronic equipment. As shown in Fig. 8a,

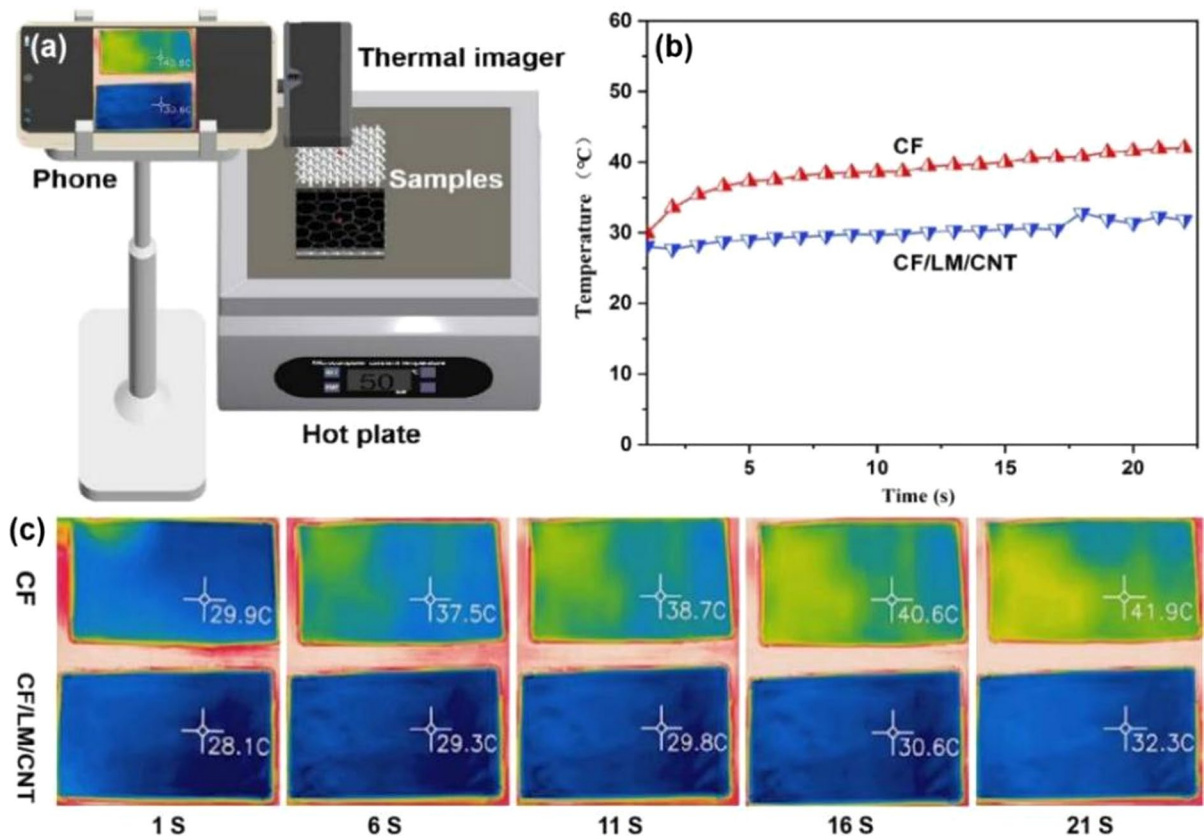
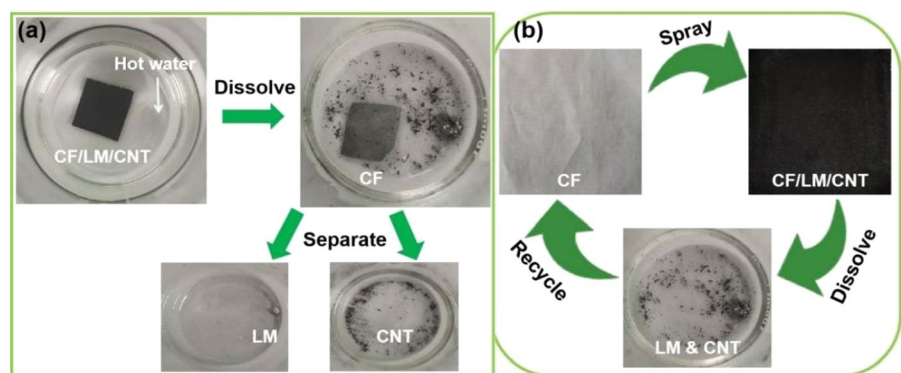


Fig. 7 **a** A self-made experimental setup for investigating the thermal insulation behavior of CF/LM/CNT; **b** Thermal insulation curves of CF/LM/CNT and CF samples; **c** The captured Infrared images of CF/LM/CNT and CF at different time intervals

Fig. 8 **a** Dissolving of the as-prepared CF/LM/CNT in hot water, and separation of LM and CNT; **b** A cycle route of a reconfigurable CF/LM/CNT sample



the as-prepared CF/LM/CNT fabric can be dissolved in hot water under oscillation and stirring at 100 °C. The LM and CNT were successfully separated afterwards. Figure 8b shows a cycle route of a reconfigurable CF/LM/CNT fabric sample. This typical example proves that the surface-spraying

strategy is green and environmentally friendly. In a word, the as-prepared fabric-based material have great potential in effective EMI shielding and rapid heat dissipation, which can fill an important gap of flexible recyclable electronic products.

Conclusion

Multilayered cotton fabric (CF/LM/CNT) was successfully fabricated by multi-layer spraying and mechanical compression. The double face-sprayed CF/LM/CNT exhibited a highly conductive behavior with an electrical resistance of 0.07 Ω , and outstanding electro-magnetic shielding capability of about 85 dB (which outperform those of most reported EMI shielding materials). Introduction of LM and CNT play an essential role in the enhanced electromagnetic shielding capability of CF/LM/CNT. The value of absorption EMSE (SE_A) for CF/LM/CNT was higher than that of the reflection EMSE (SE_R), revealing the absorption-dominant electromagnetic shielding mechanism. Moreover, the prepared CF/LM/CNT exhibited superior heat dissipation and thermal insulation performances. The as-prepared CF/LM/CNT turned out to be recyclable and reconfigurable. This work provides a facile and scalable method to fabricate multifunctional conductive textiles for flexible and wearable electronics.

Acknowledgments J.W. and Y.W. contributed equally to this work.

Funding This research was supported by the Key Project of the Education Department of Hubei Province (D20211702), the State Key Laboratory of New Textile Materials and Advanced Processing Technologies (No. FZ2020016), and the Key Laboratory of Jiangsu R&D Center of the Ecological Textile Engineering & Technology, Yancheng Polytechnic College (No. YGKF202015).

Declarations

Conflict of interest We declare that we have no financial and personal relationships with other people or organizations that can inappropriately influence our work.

References

- Bhattacharjee Y, Chatterjee D, Bose S (2018) Core-multishell heterostructure with excellent heat dissipation for electromagnetic interference shielding. *ACS Appl Mater Inter* 10:30762–30773. <https://doi.org/10.1021/acsami.8b10819>
- Bi S, Hou L, Lu Y (2021) An integrated wearable strain, temperature and humidity sensor for multifunctional monitoring. *Compos Part A Appl Sci Manuf* 149:106504. <https://doi.org/10.1016/j.compositesa.2021.106504>
- Chen Y, Li J, Li T, Zhang L, Meng F (2021) Recent advances in graphene-based films for electromagnetic interference shielding: review and future prospects. *Carbon* 180:163–184. <https://doi.org/10.1016/j.carbon.2021.04.091>
- Cheng D, He M, Ran J, Cai G, Wu J, Wang X (2018) Depositing a flexible substrate of triangular silver nanoplates onto cotton fabrics for sensitive SERS detection. *Sens Actuat B-Chem* 270:508–517. <https://doi.org/10.1016/j.snb.2018.05.075>
- Cheng D, Bai X, Pan J, Wu J, Ran J, Cai G (2020a) Wang X In situ hydrothermal growth of Cu NPs on knitted fabrics through polydopamine templates for heating and sensing. *Chem Eng J* 382:123036. <https://doi.org/10.1016/j.cej.2019.123036>
- Cheng D, Liu Y, Zhang Y, Ran J, Bi S, Deng Z, Wang X (2020b) Polydopamine-assisted deposition of CuS nanoparticles on cotton fabrics for photocatalytic and photothermal conversion performance. *Cellulose* 27(14):8443–8455. <https://doi.org/10.1007/s10570-020-03358-5>
- Cheng D, Bai X, Pan J, Ran J, Wu J, Bi S, Wang X (2020c) Immobilizing reduced graphene oxide on polydopamine-templated PET fabrics for UV protection, electrical conduction and application as wearable sensors. *Mater Chem Phys* 241:122371. <https://doi.org/10.1016/j.matchemphys.2019.122371>
- Dobosz A, Novakovic R, Gancarz T (2021) Liquid metals: thermophysical properties of alloys from the Ga-Sn-Zn system. *J Mol Liq* 343:117646. <https://doi.org/10.1016/j.molliq.2021.117646>
- Dong T, Zhang X, Wang P, Chen HS, Yang P (2020) Formation of Ni-doped MoS₂ nanosheets on N-doped carbon nanotubes towards superior hydrogen evolution. *Electrochim Acta* 338:135885. <https://doi.org/10.1016/j.electacta.2020.135885>
- Guo J, Cheng J, Tan H, Qiao Z, Yang J, Liu W (2019) Ga-based liquid metal: a novel current-carrying lubricant. *Tribol Int* 135:457–462. <https://doi.org/10.1016/j.triboint.2019.03.039>
- Guo Z, Ren P, Dai Z, Zong Z, Zhang F, Jin Y, Ren F (2021) Construction of interconnected and oriented graphene nanosheets networks in cellulose aerogel film for high-efficiency electromagnetic interference shielding. *Cellulose* 28(5):3135–3148. <https://doi.org/10.1007/s10570-021-03722-z>
- Hao Y, Gao J, Lv Y, Liu J (2022) Low melting point alloys enabled stiffness tunable advanced materials. *Adv Funct Mater* 32:2201942. <https://doi.org/10.1002/adfm.202201942>
- He J, Shi F, Wu J, Ye J (2021) Shape transformation mechanism of gallium–indium alloyed liquid metal nanoparticles. *Adv Mater Interfaces* 8:2001874. <https://doi.org/10.1002/admi.202001874>
- Hu L, Kang Z (2021) Enhanced flexible polypropylene fabric with silver/magnetic carbon nanotubes coatings for electromagnetic interference shielding. *Appl Surf Sci* 568:150845. <https://doi.org/10.1016/j.apsusc.2021.150845>
- Hu Y, Jensen JO, Zhang W, Cleemann LN, Xing W, Bjerrum NJ, Li Q (2014) Hollow spheres of iron carbide nanoparticles encased in graphitic layers as oxygen reduction catalysts. *Angew Chem Int Edit* 126:3749–3753. <https://doi.org/10.1002/ange.201400358>

- Ji K, Zhao H, Zhang J, Chen J, Dai Z (2014) Fabrication and electromagnetic interference shielding performance of open-cell foam of a Cu–Ni alloy integrated with CNTs. *Appl Surf Sci* 311:351–356. <https://doi.org/10.1016/j.apsusc.2014.05.067>
- Lee TW, Lee SE, Jeong YG (2016) Carbon nanotube/cellulose papers with high performance in electric heating and electromagnetic interference shielding. *Compos Sci Technol* 131:77–87. <https://doi.org/10.1016/j.compscitech.2016.06.003>
- Liao SY, Wang XY, Li XM, Wan YJ, Zhao T, Hu YG, Wong CP (2021) Flexible liquid metal/cellulose nanofiber composite film with excellent thermal reliability for highly efficient and broadband EMI shielding. *Chem Eng J* 422:129962. <https://doi.org/10.1016/j.cej.2021.129962>
- Luo Z, Ji C, Yin L, Zhu G, Xu BB, Wang Y, Luo K (2020) A Ga–Sn liquid metal-mediated structural cathode for Li–O₂ batteries. *Mater Today Energy* 18:100559. <https://doi.org/10.1016/j.mtener.2020.100559>
- Mondal S, Ganguly S, Das P, Bhawal P, Das TK, Nayak L, Das NC (2017) High-performance carbon nanofiber coated cellulose filter paper for electromagnetic interference shielding. *Cellulose* 24(11):5117–5131. <https://doi.org/10.1007/s10570-017-1441-4>
- Mwesigye A, Yılmaz İH (2020) Thermal and thermodynamic benchmarking of liquid heat transfer fluids in a high concentration ratio parabolic trough solar collector system. *J Mol Liq* 319:114151. <https://doi.org/10.1016/j.molliq.2020.114151>
- Peng H, Jiang Y, Chen S (2016) Efficient vacuum-free-processed quantum dot light-emitting diodes with printable liquid metal cathodes. *Nanoscale* 8:17765–17773. <https://doi.org/10.1039/C6NR05181B>
- Qin W, Guo R (2015) Metallization of polyester fabric by autocatalytic copper plating process using glyoxylic acid as a reducing agent. *Fibers Polym* 16:1671–1675. <https://doi.org/10.1007/s12221-015-4943-4>
- Ran J, Chen H, Bi S, Guo Q, Deng Z, Cai G, Wang X (2020) One-step in-situ growth of zeolitic imidazole frameworks-8 on cotton fabrics for photocatalysis and antimicrobial activity. *Cellulose* 27:10447–10459. <https://doi.org/10.1007/s10570-020-03483-1>
- Sankaran S, Deshmukh K, Ahamed MB, Pasha SK (2018) Recent advances in electromagnetic interference shielding properties of metal and carbon filler reinforced flexible polymer composites: a review. *Compos Part A Appl Sci Manuf* 114:49–71. <https://doi.org/10.1016/j.compositesa.2018.08.006>
- Wang F, Bai C, Yu Y (2021) Boron nitride nanocomposites for microwave absorption: a review. *Mater Today Nano* 13:100108. <https://doi.org/10.1016/j.mtnano.2020.100108>
- Wang Y, Wang W, Ding X, Yu D (2020) Multilayer-structured Ni-Co-Fe-P/polyaniline/polyimide composite fabric for robust electromagnetic shielding with low reflection characteristic. *Chem Eng J* 380:122553. <https://doi.org/10.1016/j.cej.2019.122553>
- Wei C, Fei H, An Y, Tao Y, Feng J, Qian Y (2019) Uniform Li deposition by regulating the initial nucleation barrier via a simple liquid-metal coating for a dendrite-free Li–metal anode. *J Mater Chem A* 7:18861–18870. <https://doi.org/10.1039/C9TA06663B>
- Xu X, Wu S, Cui J, Yang L, Liu D, Zhang Y, Sun D (2021) Insights into the microstructures and reinforcement mechanism of nano-fibrillated cellulose/MXene based electromagnetic interference shielding film. *Cellulose* 28(6):3311–3325. <https://doi.org/10.1007/s10570-021-03765-2>
- Yang Y, Chen S, Li W, Li P, Ma J, Li B, Liu Y (2020) Reduced graphene oxide conformally wrapped silver nanowire networks for flexible transparent heating and electromagnetic interference shielding. *ACS Nano* 148:754–8765. <https://doi.org/10.1021/acsnano.0c03337>
- Yao B, Xu X, Li H, Han Z, Hao J, Yang G, Wang H (2021) Soft liquid-metal/elastomer foam with compression-adjustable thermal conductivity and electromagnetic interference shielding. *Chem Eng J* 410:128288. <https://doi.org/10.1016/j.cej.2020.128288>
- Yu D, Liao Y, Song Y, Wang S, Wan H, Zeng Y, He Z (2020) A super-stretchable liquid metal foamed elastomer for tunable control of electromagnetic waves and thermal transport. *Adv Sci* 7:2000177. <https://doi.org/10.1002/adv.202000177>
- Zhang J, Li J, Tan G, Hu R, Wang J, Chang C, Wang X (2017) Thin and flexible Fe–Si–B/Ni–Cu–P metallic glass multilayer composites for efficient electromagnetic interference shielding. *ACS Appl Mater Inter* 9:42192–42199. <https://doi.org/10.1021/acsmi.7b12504>
- Zhang M, Zhang P, Zhang C, Chang H, Rao W (2020) Porous and anisotropic liquid metal composites with tunable reflection ratio for low-temperature electromagnetic interference shielding. *Appl Mater Today* 19:100612. <https://doi.org/10.1016/j.apmt.2020.100612>
- Zhao H, Hou L, Lu Y (2016) Electromagnetic shielding effectiveness and serviceability of the multilayer structured cuprammonium fabric/polypyrrole/copper (CF/PPy/Cu) composite. *Chem Eng J* 297:170–179. <https://doi.org/10.1016/j.cej.2016.04.004>
- Zhao H, Hou L, Bi S, Lu Y (2017) Enhanced X-band electromagnetic-interference shielding performance of layer-structured fabric-supported polyaniline/cobalt–nickel coatings. *ACS Appl Mater Inter* 9:33059–33070. <https://doi.org/10.1021/acsmi.7b07941>

Publisher's Note Springer Nature remains neutral with regard to jurisdictional claims in published maps and institutional affiliations.

Springer Nature or its licensor holds exclusive rights to this article under a publishing agreement with the author(s) or other rightsholder(s); author self-archiving of the accepted manuscript version of this article is solely governed by the terms of such publishing agreement and applicable law.